Direct Simulation of High Reynolds Number Flows of Complex Geometries

Kunio Kuwahara* **and Satoko Komurasaki****
* The Institute of Space and Astronautical Science
Yoshinodai, Sagamihara-shi, Kanagawa 229-8510, Japan
** Dept. of Mathematics, College of Science and Technology, Nihon Univ.
Kanda-Surugadai, Chiyoda-ku, Tokyo 101-8308, Japan

ABSTRACT– Incompressible high-Reynolds-number flows are simulated by solving the Navier-Stokes equations. A finite-difference method with third-order upwinding are employed without using any turbulence model. Multi-directional formulation is applied for improved accuracy. Validity of this method is discussed. Examples are presented to show the applicability of the present approach to variety of problems.

Keywords: Direct simulation; Navier-Stokes equations; Multi-directional finite-difference.

1. INTRODUCTION

Many of high-Reynolds-number, turbulence simulations have been based on Reynolds-averaged Navier-Stokes equations using a turbulence model. Some use a large-eddy simulation based on a Smagorinsky-type model (Deardorff, 1970). However, a usual turbulence model or a large-eddy simulation is not suitable for high-Reynolds-number-flow computation because, there, the effect of turbulence mixing is usually replaced by second-order diffusion. This diffusion is similar to viscous diffusion. It means that we are simply computing a locally low-Reynolds-number flow.

There are some real direct numerical simulation in which most of the small-scale structure are resolved, but the computations can be done only at relatively small Reynolds numbers. We can not use enough grid points for high-Reynolds-number flows of practical interest. We have rather to use a very coarse grid system. In many applications, large structures are most important. What we want to do is to capture the large-scale structure using a coarse grid system.

On the other hand, quit a few simulations (see Kuwahara, 1999), show that large structures of high-Reynolds-number, turbulent flow can be captured using relatively coarse grid, if the numerical instability, usually unavoidable for high-Reynolds-number-flow simulation, is suppressed. Most successful simulations in these approaches are based on the third-order upwind formulation (Kawamura and Kuwahara, 1984). An approach similar in philosophy but different in method is adopted by Boris et. al. (1992).

In the present paper, we summarize the third-order upwind scheme for high-Reynolds-number-flow computations. To increase the accuracy, we have developed multi-directional finite-difference method.

2. COMPUTATIONAL METHOD

The governing equations are the incompressible Navier-Stokes equations. In three-dimensional Cartesian coordinates system, they are as follows:

$$\frac{\partial u_j}{\partial x_j} = 0, \tag{1}$$

$$\frac{\partial u_i}{\partial t} + u_j \frac{\partial u_i}{\partial x_j} = -\frac{\partial p}{\partial x_i} + \frac{\partial}{\partial x_j}\left\{\frac{1}{Re}\left(\frac{\partial u_i}{\partial x_j} + \frac{\partial u_j}{\partial x_i}\right)\right\}. \tag{2}$$

For high-Reynolds-number flows, time-dependent computations are required owing to the strong unsteadiness. A finite-difference method is employed to solve the basic equations computationally. These equations are solved by using projection method (Chorin, 1968, and Takami and Kuwahara, 1974). This method can be written in the following form when it is applied to the above equations:

$$\boldsymbol{w} + \mathrm{grad}p = \boldsymbol{F}, \tag{3}$$

$$\mathrm{div}\boldsymbol{w} = 0, \tag{4}$$

where

$$\boldsymbol{w} = w_i, \quad \boldsymbol{F} = F_i \quad (i = 1, 2, 3),$$

$$w_i = \frac{\partial u_i}{\partial t}, \tag{5}$$

$$F_i = -u_j \frac{\partial u_i}{\partial x_j} + \frac{\partial}{\partial x_j}\left\{\frac{1}{Re}\left(\frac{\partial u_i}{\partial x_j} + \frac{\partial u_j}{\partial x_i}\right)\right\}, \tag{6}$$

The Helmholtz's decomposition works.

$$\boldsymbol{w}^{\nu} = \boldsymbol{F} - \mathrm{Grad}p^{\nu}, \tag{7}$$

$$p^{\nu+1} = p^{\nu} - \varepsilon \left(\mathrm{Div}\boldsymbol{w}^{\nu} + \frac{1}{\Delta t}\mathrm{Div}\boldsymbol{u} \right), \qquad (8)$$

where the index ν denotes the νth iterations and ε is a relaxation constant. Symbols Grad and Div are suitable difference approximations to the operators grad and div. The last term with $1/\Delta t$ in eq.(8) is the correction term for preventing the accumulation of the error in $\boldsymbol{w}$. If p and ε are regarded as the temperature and time increment, eq.(8) is considered to be the heat equation discretized by the Euler explicit method. For its stability, the value of ε is obtained. Equation (8) becomes Poisson equation for the pressure

$$\mathrm{Div}(\mathrm{Grad}p) = \mathrm{Div}\boldsymbol{F} + \frac{1}{\Delta t}\mathrm{Div}\boldsymbol{u} \qquad (9)$$

after the convergence when $p^{\nu+1}$ is equal to p^{ν}. Although this method is essentially the same as the MAC method, the effect of the compressibility due to the temperature difference is correctly evaluated in this formulation.

All the spatial derivative terms are represented by the central difference approximation except for the convection terms. For the convection terms, the third-order upwind difference is used to stabilize the computation. This is the most important point for high-Reynolds-number computations and the detail is given below.

Strong numerical instability caused by the aliasing error occurs at high Reynolds numbers, owing to the non-linear convection terms, if enough grid points are not used to resolve the small-scale structures. When digitizing a continuous function into a finite number of the values, it is very important to filter out the high-frequency part of the original function which can not be resolved by the digital system. If not, aliasing error makes the approximation meaningless.

Usually a turbulence model or a large eddy simulation is used to get rid of this instability. The diffusion coefficients increased by the added turbulent viscosity reduce the aliasing error and suppress the numerical instability. In most of the models, this diffusion has the same form as the viscous diffusion and the diffusion coefficient is usually much larger than that of the viscous diffusion. Therefore, the effect of physical diffusion is concealed, resulting no dependency of the flow on the Reynolds number is captured.

Another way to stabilize the computation is to use an upwind scheme. The first-order upwind scheme is widely used because of the very good stability but the leading numerical error caused by this upwinding is second order and similar to the physical diffusion. This should be avoided because of the same reason just mentioned above.

The second-order upwind scheme has a dispersion type leading error, which makes the computation unstable generally.

For the discretization of the non-linear convection terms, it has special importance for stable computation whether the order of accuracy is odd or even. In case of even order of accuracy, the leading numerical-error term is the odd-order derivative which is dispersive. Once some error is created, the error never diffuses but moves around in the computational domain until the computation blows up. Eventually no stable solution can be obtained in this case. On the other hand, in case of odd order of accuracy, the leading error term is the even-order derivative which is diffusive. This makes the computation very stable by reducing the aliasing error well.

A third-order upwind scheme has been found to be most suitable for high-Reynolds-number-flow computation. The leading numerical error terms are the fourth-order derivative terms, where the effects of the second-order numerical diffusions are carefully removed. The numerical diffusion of forth-order derivatives is of short range and does not conceal the effect of molecular diffusion but well stabilizes the computation.

One simple explanation why the fourth-order diffusion does not conceal the effect of second-order diffusion is as follows. A finite-difference representation of the fourth-order diffusion term is as follows:

$$(u_{k+2} - 4u_{k+1} + 6u_k - 4u_{k-1} + u_{k-2})/(\Delta x)^4 \qquad (10)$$

This can be written as,

$$\frac{4}{(\Delta x)^2}\left(\frac{u_{k+2} - 2u_k + u_{k-2}}{(2\Delta x)^2} - \frac{u_{k+1} - 2u_k + u_{k-1}}{(\Delta x)^2} \right). \qquad (11)$$

The two terms in eq.(11) represent the second-order diffusion and their effects are canceled each other except near the point k. This means fourth-order diffusion is very independent from second-order diffusion. In general, the effects of lower-order diffusion are not concealed by higher-order diffusion.

Similarly, fifth-order upwinding is possible and some computations have been done but it requires seven points in each direction to approximate the local derivative. This means to require a wider range of analyticity to the solution of the equations. High-Reynolds-number flows are not so analytical, therefore it is not necessarily better than third-order unwinding.

There are several third-order upwind schemes. We use the following scheme. Initially, the one-sided second-order finite difference approximation is employed for the convection terms.

$$u\frac{\partial u}{\partial x} \approx \begin{cases} u_k \cdot \left(\frac{3u_k - 4u_{k-1} + u_{k-2}}{2\Delta x} \right) & (u_k > 0) \\ u_k \cdot \left(\frac{-u_{k+2} + 4u_{k+1} - 3u_k}{2\Delta x} \right) & (u_k < 0) \end{cases} \qquad (12)$$

We can rewrite the above equations to a symmetrical

form by using the formula:

$$\frac{u_k+|u_k|}{2}=\begin{cases} u_k & (u_k>0) \\ 0 & (u_k<0) \end{cases},$$

$$\frac{u_k-|u_k|}{2}=\begin{cases} 0 & (u_k>0) \\ u_k & (u_k<0) \end{cases}.$$

Then, eq.(12) can be written

$$\begin{aligned} u\frac{\partial u}{\partial x} &\approx \frac{u_k+|u_k|}{2}\left(\frac{3u_k-4u_{k-1}+u_{k-2}}{2\Delta x}\right) \\ &+ \frac{u_k-|u_k|}{2}\left(\frac{-u_{k+2}+4u_{k+1}-3u_k}{2\Delta x}\right). \end{aligned}$$

Finally, we get

$$\begin{aligned} u\frac{\partial u}{\partial x} &\approx u_k\cdot\frac{-u_{k+2}+4(u_{k+1}-u_{k-1})+u_{k-2}}{4\Delta x} \\ &+|u_k|\cdot\frac{u_{k+2}-4u_{k+1}+6u_k-4u_{k-1}+u_{k-2}}{4\Delta x}. \end{aligned} \tag{13}$$

If the first and second terms of eq.(13) are developed into Taylor series, they become respectively,

$$u\frac{\partial u}{\partial x}-\frac{1}{3}(\Delta x)^2u\frac{\partial^3u}{\partial x^3}+O((\Delta x)^4)$$

and

$$\frac{1}{4}(\Delta x)^3u\frac{\partial^4u}{\partial x^4}+O((\Delta x)^5). \tag{14}$$

Therefore, the leading error of eq.(13) is order $(\Delta x)^3$ and its coefficient includes third-order derivative. As mentioned above, odd order-derivative is not desirable, but this error term is eliminated if the first term of eq.(13) is replaced by

$$u_k\cdot(-u_{k+2}+8(u_{k+1}-u_{k-1})+u_{k-2})/12\Delta x. \tag{15}$$

As a result, the present third-order upwind scheme is represented by five grid points as follows:

$$\begin{aligned} u\frac{\partial u}{\partial x} &\approx u_k\cdot\frac{-u_{k+2}+8(u_{k+1}-u_{k-1})+u_{k-2}}{12\Delta x} \\ &+|u_k|\cdot\frac{u_{k+2}-4u_{k+1}+6u_k-4u_{k-1}+u_{k-2}}{12\Delta x}. \end{aligned} \tag{16}$$

This scheme is called Kawamura-Kuwahara scheme (1984). There is another version of third order upwind schemes for example as follows:

$$\begin{aligned} u\frac{\partial u}{\partial x} &\approx u_k\cdot\frac{-u_{k+2}+8(u_{k+1}-u_{k-1})+u_{k-2}}{12\Delta x} \\ &+\alpha|u_k|\cdot\frac{u_{k+2}-4u_{k+1}+6u_k-4u_{k-1}+u_{k-2}}{12\Delta x}, \end{aligned} \tag{17}$$

where α is chosen suitably. We compared Kawamura-Kuwahara scheme, UTOPIA and QUICK schemes (Leonard, 1979) by the energy spectrum in one-dimensional Burgers turbulence and found the above Kawamura-Kuwahara scheme is the best (fig.1). When we use a very fine grid as 4096 points, the three schemes agree completely with each other and theoretical prediction. However, with reducing the number of grid points, the difference become clear. Only the present method give the good agreement with the result of very fine computations.

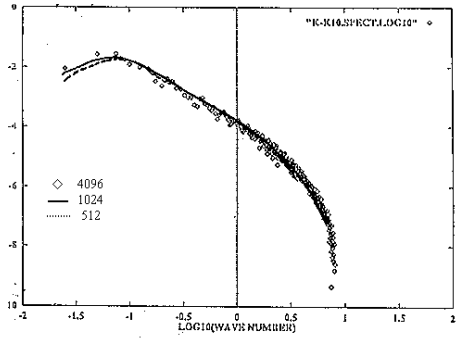

(a) The present scheme (Kawamura-Kuwahara)

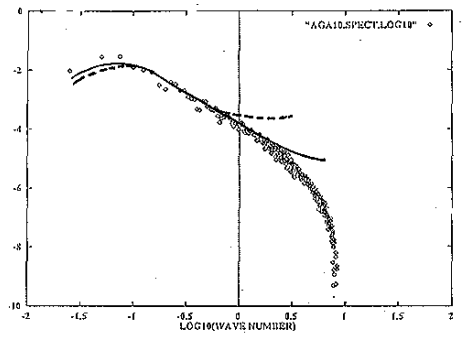

(b) UTOPIA

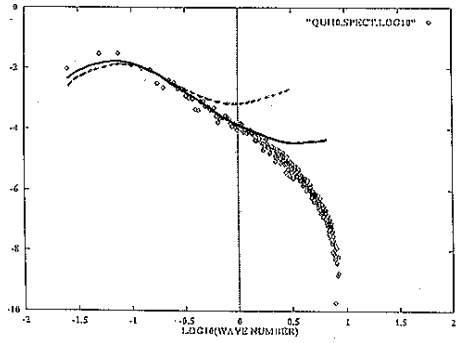

(c) QUICK

Fig.1 Energy spectrum for Burgers turbulence.

There is another important problem in high-order upwind schemes. That is, the accuracy decreases when the flow direction is not well parallel to one of the coordinate lines. If we use generalized coordinate system, near the boundary, the flow direction and one of the coordinate lines are almost parallel, and this problem is not serious. However, in general, flow direction is not always parallel to a coordinate line and the problem become very important.

To overcome this problem we introduced the multi-directional upwind method. This method is summarized as follows:

In case of 2-dimensional computation, when structured grid points are given, the black points in fig.2(a) are usually used to approximate the derivatives at the central point (system A). If we introduce the other 45 degrees-rotated local grid points, the white ones in fig.2(b), which can be used to approximate the derivatives at the central point (system B). In order to improve the derivative value at the central point, we mix the derivative values calculated from both systems (A and B) at a proper ratio. We adopt the ratio A : B = 2/3 : 1/3. Using this ratio, for example, resulting finite-difference scheme for the Laplacian coincides with the well-known 9-points formula with forth-order accuracy. This method improves the rotational invariance of the coordinate system. Then those flows where flow direction is not parallel to the grid direction are better simulated.

In case of 3-dimensional computation, we introduce three different grid systems. Each grid system is obtained by rotating ordinary one (system A) around one axis. For example, one of those systems, system B (x'-y'-z) is shown in fig.2. In the same way as 2-dimensional computation, white circle points are used instead of black ones on the x-y plane, and ordinary ones in the z direction. Other grid systems are also introduced similarly. Thus we can obtain three different values at the same point, and they are averaged, since any physical phenomena are equivalent in each grid system. The rotational invariance of the coordinate system can be improved by means of this method.

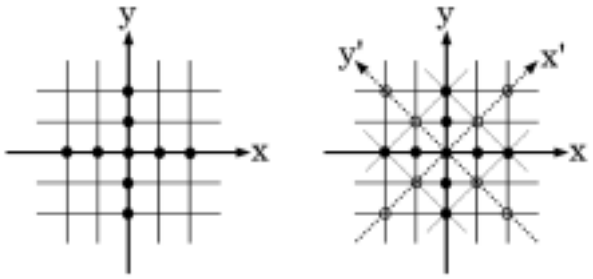

(a) system A (b) system B

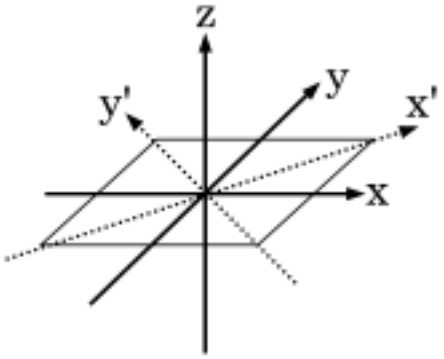

(c) system B: x'-y'-z

Fig.2 Grid for multi-directional scheme

For all the spatial derivatives, the multi-directional finite-difference method is used. This method has another advantage. In MAC method, usually staggered mesh is used to remove the unphysical oscillation of the pressure. This oscillations is caused by the decoupling of the computed values within the nearest two points. These values couples more tightly with the second nearest points. This decoupling become less if we use third-order upwind scheme because of the five-point differencing, but there remains some. However, if we use multi-directional finite-difference method, every point becomes tightly coupled and the oscillation disappears. Therefore, a non-staggered mesh system is employed where the defined positions of velocity and pressure are coincident.

For the temporal integration of the Navier-Stokes equations, the Crank-Nicolson implicit scheme is utilized. This scheme has second-order accuracy in time. These equations and the Poisson equation are iteratively solved at each time step by the successive over relaxation (SOR) coupled with a multi-grid method.

3. COMPUTATIONAL RESULTS

3.1. CIRCULAR CYLINDER

The dependence of the drag coefficients on Reynolds numbers is shown in fig.3. The number of grid points are 32*16, 64*32, 128*64. If the Reynolds number is less than 100, all the computations and experiments agree very well. At high Reynolds numbers even 64*32 computation can capture the drag crisis qualitatively. The 128*64 computations agrees much better with the experiments as expected.

The drag sharply decreases at about Reynolds number 400000, which is called drag crisis, is well captured even using this coarse grid. Instantaneous and time-averaged flow patterns clearly show the difference as shown in fig.4. After drag crisis, flow separation delays and the wake becomes narrower, which makes the drag less.

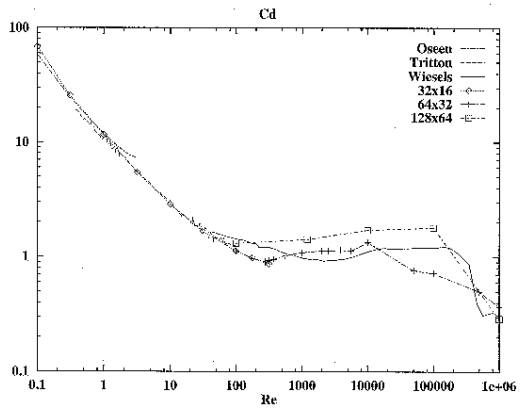

Fig.3 Drag coefficients of circular cylinder (Kuwahara, 1999)

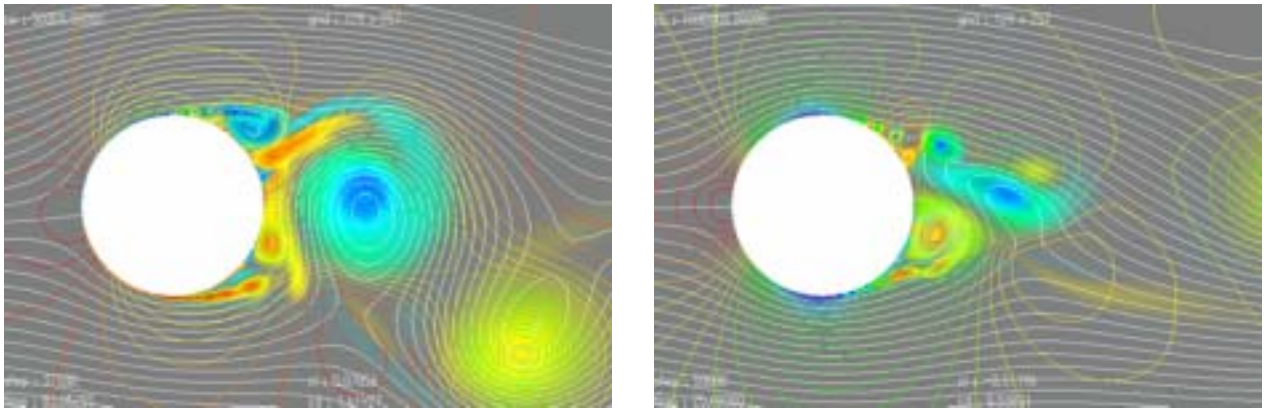

(a) Re=50000, before drag crisis (b) Re=1000000, after drag crisis

Fig.4 Flow past a circular cylinder, streamlines and pressure contours, background color shading shows, the vorticity distribution. Instantaneous flow field, 128*256 grid system.

3.2. REARRANGEMENT OF KARMAN VORTEX STREET

Two-dimensional flows past a bluff body usually accompany a Karman Vortex street. It rearranges itself and makes another Karman Vortex street of different wave length. However, this phenomenon occurs far beyond the body. Therefore, to simulate this, we must include a long wake region in the computational domain. We need about 1000 times length of the body size. However, in even two-dimensional computation, we can use several thousands grid points in one direction. This means the body should be represented by several grid points. This becomes possible by using the present multi-directional finite-difference method. Figure 5 shows the Karman Vortex street and its rearrangement. The body is represented by only three grid points. Total number of the grid points is 2059*257. The upper part of figure is the velocity component perpendicular to the flow direction.

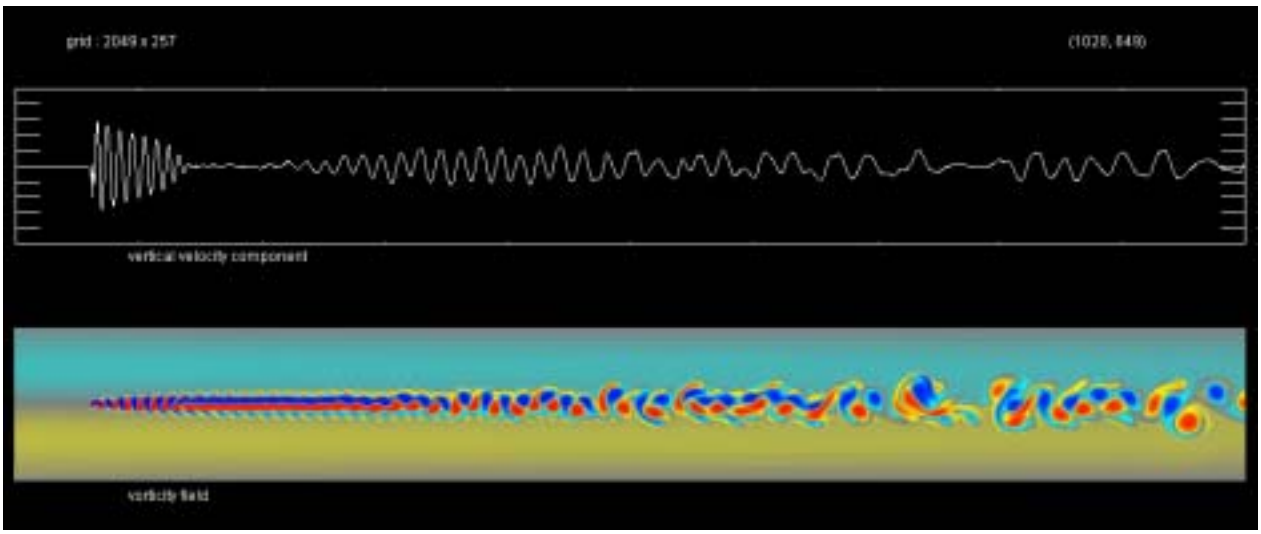

Fig.5 Rearrangement of karman vortex street. 2058*256 Cartesian grid system.

3.3. FLOW AROUND AN AIRFOIL

Flow around an airfoil is a standard problem, but unsteady computations have rarely been done. At high angle of attack, the flow becomes very unsteady and to understand the flow well we need an unsteady simulation. For airfoil simulation, C-grid is usually used to avoid the trailing edge singularity. To make C-grid is not easy for very high angle of attack, and this is another reason of the difficulty to simulate the flow at very high angle of attack. Also C-grid needs unnecessarily concentrated grid points in the near wake region beginning from the trailing edge. This make the computation more unstable. On the other hand O-grid is, in every sense, much better if the computation converges. The multi-directional finite-difference method makes the computation very stable even near the singular points. Computed lift coefficients agree well with experiments.

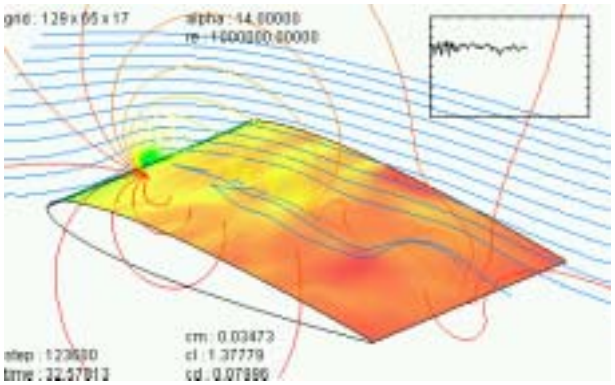

(a) Angle of attack 14 degrees

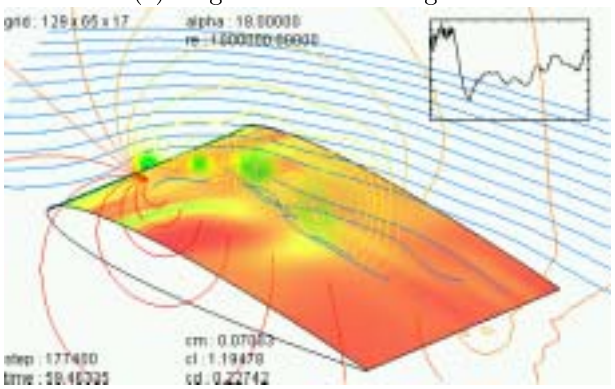

(b) Angle of attack 18 degrees

Fig.6 Flow around NACA0012 airfoil at Re=1000000, 128*64*16 O-grid system, instantaneous streamlines, pressure contours, pressure shading on the airfoil. (Kuwahara and Komurasaki, 2001)

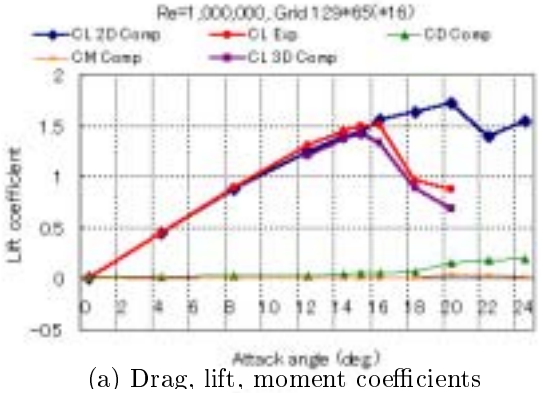

(a) Drag, lift, moment coefficients

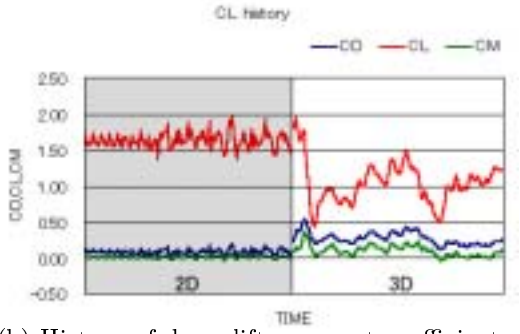

(b) History of drag, lift, moment coefficients at attack angle 18 degrees

Fig.7 Computed force coefficients around NACA0012 airfoil.

Figure 7(a) shows the drag, lift and moment coefficients cd, cl, cm in 2D and 3D computations. In case of 2D computation, cl agrees perfectly well with the experimental values up to the stall angle. The lift coefficients cl become much larger than the experimental values beyond the stall angle. On the other hand, in case of 3D computation, before the stall at the attack angle 15 degrees, the lift does not change much but after the stall at attack angle 18 degrees, 3D computation quickly develops, and the lift decreases accordingly. The final results agree with the experimental ones very well (Abbott and Von Doenhoff, 1959). Figure 7(b) shows drag, history of lift and moment coefficients from 2D to 3D computation at the stall angle of 18 degrees. The left side of graph shows the result of 2D computation and the other side, 3D computation with using the result of 2D computation as the starting condition.

3.4. TRANSITION IN BLUFF BODY WAKE

It is impossible to compute transitional flow by using a turbulence model. Even large-eddy simulation can not handle this type of problem, because it assumes the flow is turbulent from the beginning. However, transition phenomena is very important at high-Reynolds number flow. In the present approach, this is not a special thing, we can compute any transitional flow without any special consideration. Figure 8 shows a flow around a protoceratopus. This is as bluff as a sphere, then the wake turbulence is very similar to the sphere. In figs.9 and 10, development of turbulence behind a sphere is shown; the sphere has impulsively started from rest. The visualization was done by showing the surface pressure of the body and the volume rendering of absolute value of the vorticity.

The number of the grid point is 288*144*144=5,971,968 in the case of sphere and 256*128*128=4,194,304 in the case of protoceratopus. These numbers are not enough to see the smallest structures but look to be good enough to see the large structure in the transitional stage.

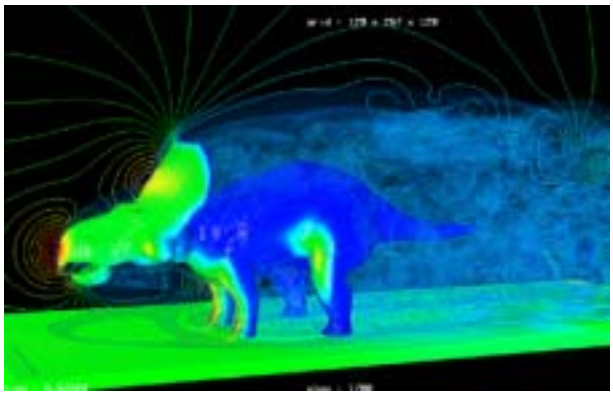

Fig.8 Flow around a protoceratopus at Re=100000, 256*128*128 grid system.

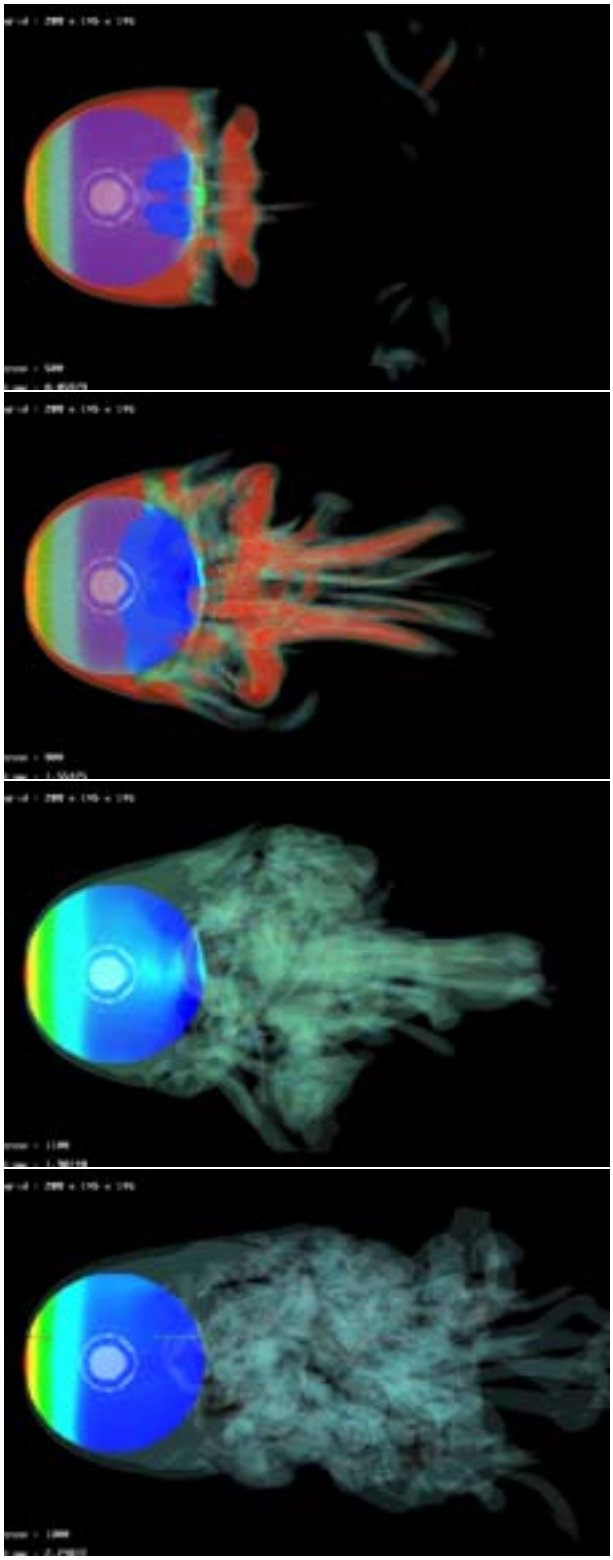

Fig.9 Development of turbulence behind a sphere at Re=20000, 288*144*144 grid system

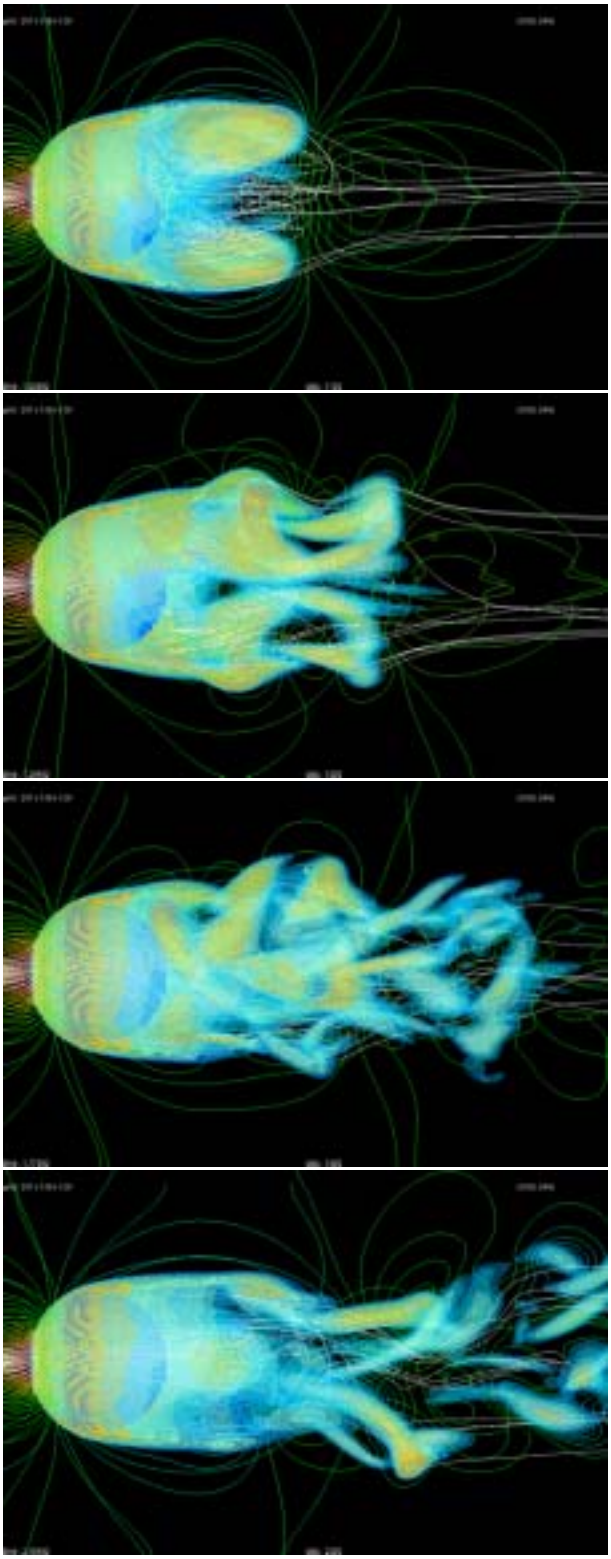

Fig.10 Development of turbulence behind a sphere at Re=2000, 256*128*128 grid system

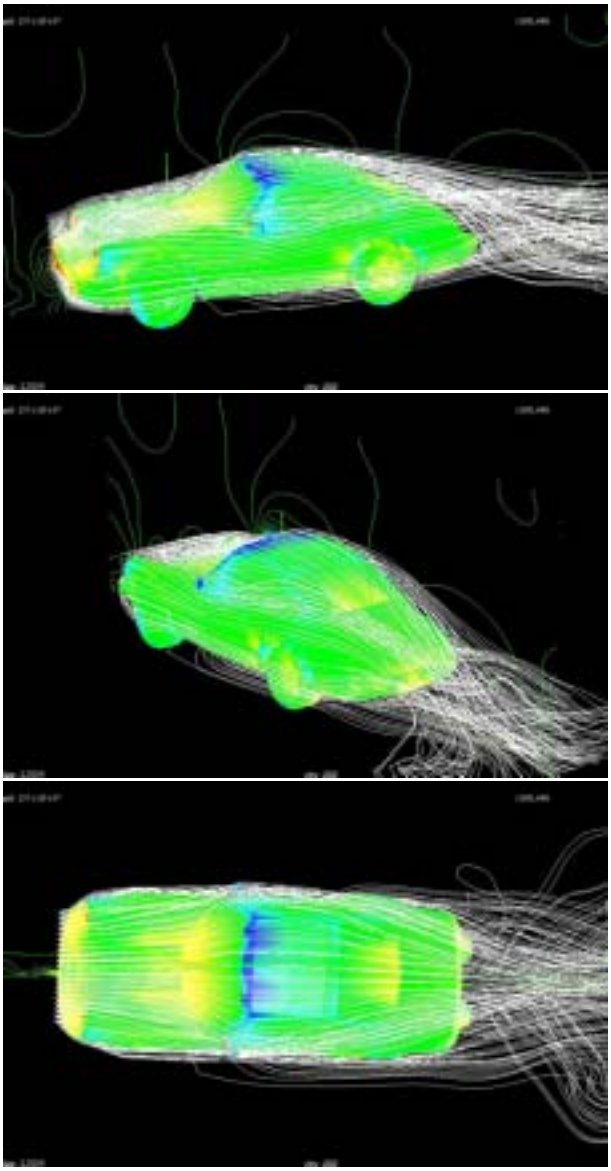

Fig.11 Flow past a car, 256*128*96 grid system. Stream lines and pressure contour lines.

3.5. SIMULATION USING A GENERALIZED COORDINATES SYSTEM MODIFIED FROM CARTESIAN COORDINATES (GCMCC)

The computation carried out by using a body-fitted coordinates for saving grid points and capturing flow mechanism exactly. The generalized coordinates system in this computation is generated by modifying Cartesian coordinates, because it is easier to generate grids and to apply to other flow problems widely. As examples, flows around one or some bluff bodies are computed in two-dimensional domain.

Figure 12(a) shows body-fitted grid which is used for computation of a flow around a circular cylinder. On the other hand, in fig.12(b), the original grid of body-fitted one in Cartesian coordinates is displayed for the same computation. In both figures, circular shadow indicates a cylinder and the number of grid points is 49*25.

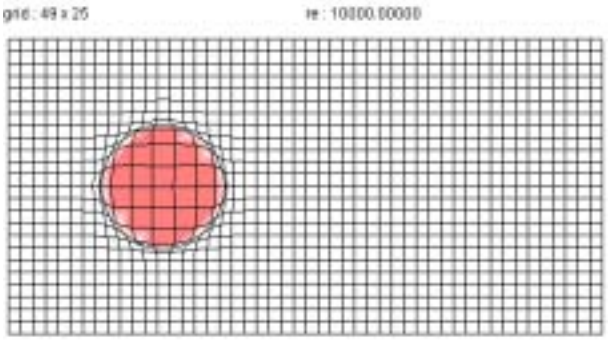

(a) Body-fitted coordinates.

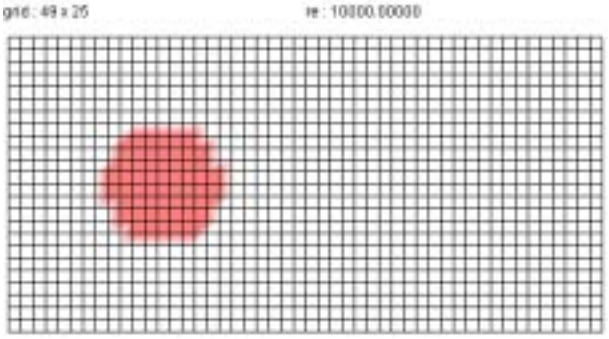

(b) Cartesian coordinates.

Fig.12 Computational grid.

In fig.13, (a) and (b) show results of 2-d computations of flow past a circular cylinder at Reynolds number = 10^4 by using GCMCC (fig.12(a)) and Cartesian coordinates (fig.12(b)) respectively. In this figure, equi-pressure contour lines and particles from the surface of cylinder are expressed.

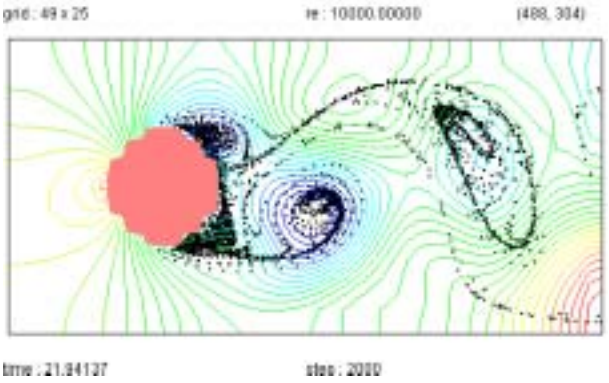

(a) Body-fitted coordinates.

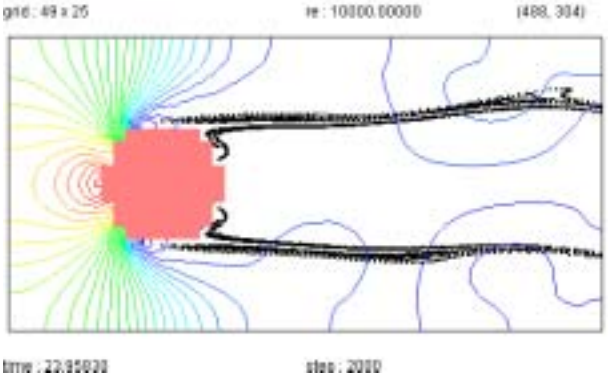

(b) Cartesian coordinates.

Fig.13 Pressure field and particles.

Figures 14 and 15 are other examples of 2-d and 3-d computations by using GCMCC grid. These results show that flow mechanisms are well captured with GCMCC even using coarse grid.

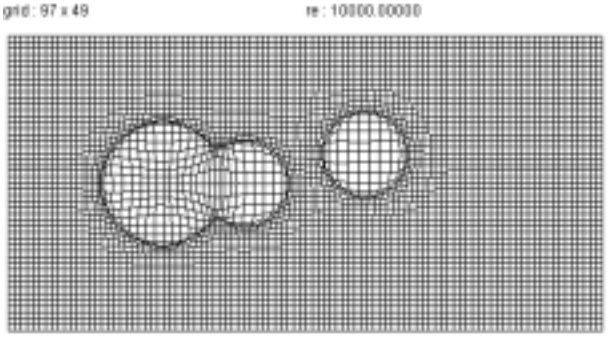

(a) Computational grid (96*48).

(b) Flow pattern. Pressure contour lines and particle path.

Fig.14 2-d flow past bluff bodies by using GCMCC grid.

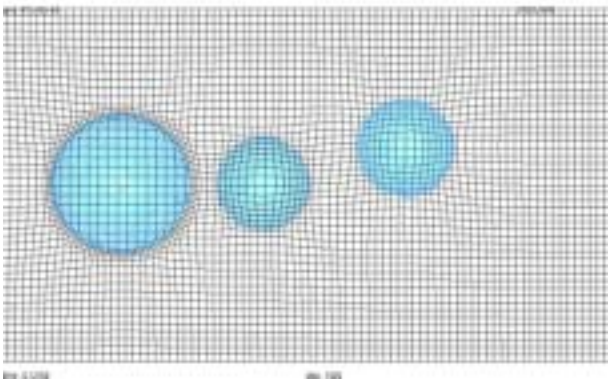

(a) Side view of computational grid (96*48*48)

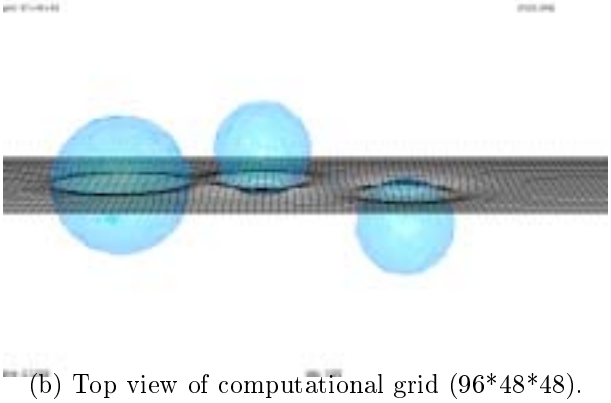

(b) Top view of computational grid (96*48*48).

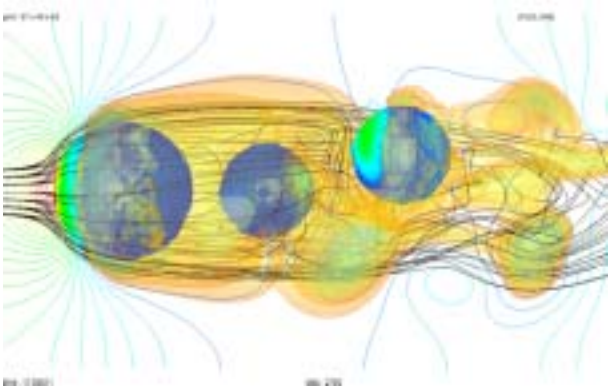

(c) Flow pattern. Stream lines, pressure contour lines and pressure volume rendering.

Fig.15 3-d flow past bluff bodies by using GCMCC grid.

4. CONCLUSION

Flows past various bodies are simulated by using Cartesian coordinates system, body-fitted coordinates and GCMCC (a generalized coordinates system modified from Cartesian coordinates).

It is becoming clear that we need not resolve the small-scale structure of high-Reynolds-number flow to capture the large structure, which is most important for application. We should not use standard models to simulate any high-Reynolds-number, turbulent flows. Only without using turbulence models we are able to capture the dependence of the flow on the Reynolds number. To avoid the numerical instability we can simply use a third-order upwind difference. Multi-directional finite-difference makes the dependence of the solution on the flow direction less and the computation more reliable.

REFERENCES

1) Abbott, I. H. and Von Doenhoff, A. E., 1959, "Theory of Wing Sections," Dover Pub., pp462

2) Boris, J.P., Grinstein, F.F., Oran, E.S. and Kolbe, R.L., 1992, "New insights into large eddy simulation," Fluid Dynamics Research 10, pp. 199-228

3) Chorin, A., J., 1968, Math. Comp. 22 pp. 745

4) Deardorff, J.W., 1970, "A Numerical Study of Three-Dimensional Turbulent Channel Flow at Large Reynolds Numbers," J. of Fluid Mechanics, Vol. 41, Part 2, pp. 453-480

5) Kawamura, T. and Kuwahara, K., 1984, "Computation of high Reynolds number flow around a circular cylinder with surface roughness," AIAA Paper 84-0340.

6) Kuwahara, K., 1999, "Unsteady Flow Simulation and Its Visualization," AIAA Paper 99-3405

7) Kuwahara, K. and Komurasaki, S., 2001, "Direct Simulation of a Flow around a Subsonic Airfoil," AIAA Paper 2001-2545

8) Leonard, B.P., 1979, "A Stable and Accurate Convective Modeling Procedure Based on Quadratic Upstream Interpolation," Computer Methods in Applied Mechanics and Engineering, Vol. 19, pp. 59-89

9) Takami, H. and Kuwahara, K., 1974, "Numerical Study of Three-Dimensional Flow within a Cubic Cavity," J. Phys. Soc. Japan, Vol. 37, No. 6